Feasibility Study of Synchrotron X-ray Diffraction and Absorption Spectroscopy for the Characterisation of NMC oxides for Li-ion Battery Cathodes

Taehoon Kim, Song Bohang, Nikolaos Baimpas, Cristian Mocuta, Dominique Thiaudiere, Lu Li and
Alexander M. Korsunsky, *Member, IAENG*

Abstract— **In lithium – transition metal oxide materials, e.g. those known as nickel-manganese-cobalt oxides, or NMC, used as active materials for battery cathodes, local distortions of the host crystal lattice during Li intercalation provide key information for understanding the origins of ageing and capacity fading. To enable the detailed characterisation of these lattice distortions, we consider the combination of advanced synchrotron-based techniques, namely, X-ray diffraction (XRD) with Rietveld refinement for precise determination of unit cell parameters and atomic positions, and X-ray absorption spectroscopy (XAS) that allows studying the oxidation state and the local environment of Mn, Ni and Co atoms. Our objective is to establish the use of this combination of techniques in transmission mode through a specially modified *in situ* coin cell that incorporates windows to enable measurements through batteries subjected to *in situ* cycling.**

Index Terms— **Lithium ion batteries, electro-chemistry, synchrotron X-ray absorption spectroscopy, EXAFS.**

I. INTRODUCTION

Lithium-ion battery is a family of the secondary battery in which lithium ions move between the cathode and anode during charging or discharging. Lithium is the lightest metal found in nature and possesses a high electrochemical

Taehoon Kim is graduate student in the Department of Engineering Science, University of Oxford, Parks Road, Oxford OX1 3PH, UK (e-mail: research.hoon@googlemail.com).

Song Bohang is graduate student in the Department of Mechanical Engineering, National University of Singapore, 9 Engineering Drive 1, Block EA#07-08, Singapore 117576 (e-mail: g0900598@nus.edu.sg).

Nikolaos Baimpas is graduate student in the Department of Engineering Science, University of Oxford, Parks Road, Oxford OX1 3PH, UK (e-mail: nikolaos.baimpas@eng.ox.ac.uk)

Cristian Mocuta is with Beamline DIFFABS, Synchrotron Soleil, Saint-Aubin, BP48, 91192 GIF-sur-YVETTE, France (e-mail: cristian.mocuta@synchrotron-soleil.fr)

Dominique Thiaudiere is with Beamline DIFFABS, Synchrotron Soleil, Saint-Aubin, BP48, 91192 GIF-sur-YVETTE, France (e-mail: dominique.thiaudiere@synchrotron-soleil.fr)

Lu Li is Professor in the Department of Mechanical Engineering, National University of Singapore, 9 Engineering Drive 1, Block EA#07-08, Singapore 117576 (email luli@nus.edu.sg).

Alexander M. Korsunsky (author for correspondence) is Professor in the Department of Engineering Science, University of Oxford, Parks Road, Oxford OX1 3PH, UK (e-mail: alexander.korsunsky@eng.ox.ac.uk, tel. +441865273043).

potential. Its high energy and power densities with its light weight make it ideal for use in battery applications. Lithium-ion batteries were first commercialised by Sony Corporation in 1991 [1]. Since then, the batteries have been widely utilized as power sources in a wide range of applications such as digital cameras, mobile phones, laptops, medical implant device, and electric vehicles. The reason of the widespread utilization is their high energy densities, high power rates and working voltage combined with flexible design, and low self-discharge. The cathode material in lithium-ion batteries is one of the core components that determine the overall performance. Materials used for electrodes in batteries host lithium ions in their structure. Typically, the electrodes in a lithium-ion battery are intercalation compounds. At present, the anode used in most lithium-ion batteries based on a graphite intercalation electrode, which stores up lithium ions between graphene layers and are also characterised by high electron conductivity.

As cathode material, lithium-rich layered materials of the type $x\text{Li}_2\text{MnO}_3\cdot(1\text{-}x)\text{LiMO}_2$ (M = Mn, Co, Ni) has received much attention in recent years owing to their higher capacity ($\sim$250 mAh/g), low cost, low toxicity, and thermal stability. It has been proposed that lithium-rich layered active materials exist as a solid solution of Li_2MnO_3 (monoclinic, C2/m) and LiMO_2 (trigonal, R-3m) [2]. The entire structure is usually represented in LiMO_2 notation. The Li_2MnO_3 region is electrochemically inactivate in terms of topotactic reactions. However, the presence of the Li_2MnO_3 structure stabilises the structure of the LiMO_2 phase during the charging process [3] and results in a rapid deintercalation of lithium with oxygen release, and thus leading to a higher capacity. It is therefore important to examine the structural stability in connection with the objective of improved material design, since the structural change of the active material has direct bearing upon the capacity fading phenomenon during charging and discharging.

In metal oxide materials of the type $\text{Li}[\text{Li}_{0.2}\text{Mn}_{0.54}\text{Ni}_{0.13}\text{Co}_{0.13}]\text{O}_2$ (also known as nickel-manganese-cobalt oxides, or NMC) used for cathodes in lithium-ion batteries, local distortions of the host crystal

lattice during Li intercalation provide key information for understanding the origins of ageing and capacity fading.

To enable detailed characterisation of these lattice distortions, we consider the combination of advanced synchrotron X-ray techniques. X-ray diffraction (XRD) followed by Rietveld refinement is suitable for precise determination of unit cell parameters and atomic positions. X-ray absorption spectroscopy (XAS) allows studying the oxidation state and the local environment of Mn, Ni and Co atoms. Our objective is to develop the use of this combination of techniques on a specially modified *in situ* coin cell that incorporates windows to allow transmission measurements through batteries subjected to *in situ* cycling.

The main questions posed in the present study were:
a) Are the methods proposed well-suited to the structural studies of NMC-type materials?
b) Are the methods sufficiently sensitive to obtain local environment data at relevant resolution?
c) Are the methods suitable for use with the *in situ* cell?

In the first part of the study we focused our attention on the analysis of NMC powders. Measurements were also conducted in transmission through modified cells, in order to establish the feasibility of this approach for *in situ* studies. Attempts were made to perform *in situ* XAS on the coin cells denoted P-4-10 (active material loading 7.08 mg), G-4-7 (5.64 mg), and G-4-8 (5.39 mg). The X-ray window on the cell was sealed with aluminium foil. The initial voltage of the specially designed cells was found to be between 0.45 V and 0.70 V, i.e. too low for charging operation. During the transportation of the cells to the synchrotron facility, loss of seal led to electrolyte leakage. The cells were re-sealed with Kapton tape within an Argon glove box, and leaked electrolyte was removed from the cell surface. XRD and XAS patterns were collected only for the G-4-7 cell.

II. EXPERIMENTAL

The two types of active materials studied were designated P-type for "pristine" (unaltered) $Li[Li_{0.2}Mn_{0.54}Ni_{0.13}Co_{0.13}]O_2$ powder, and G-type for the same powder modified with the addition of graphene, respectively. The composition of the electrodes was (active material: carbon black: PVDF) = (8:1:1). For the purposes of X-ray measurements, the powders were sandwiched between two layers of thin Kapton film. The beam spot on the powder samples was approximately 320 μm × 260 μm for both XRD and XAS. The X-ray photon energy used for XRD analysis was 11.0 keV ($\lambda = 1.127$ angstrom).

XAS spectra were collected in transmission mode at the Mn (6.537 keV), Ni (8.339 keV), and Co (7.712 keV) K-edges. Using the double crystal monochromator (DCM), the beam energy was initially tuned to 6.7 keV, 8.5 keV, and 7.85 keV, for Mn, Ni, and Co XAS analysis, respectively.

Data interpretation was performed with Demetris software package. Structural parameters were obtained by fitting within the ARTEMIS application with the FEFF 6 algorithm. Crystallographic parameters refined by the Rietveld method (GSAS) were used for EXAFS analysis.

In a separate series of *ex situ* experiments, charge-discharge cycling was performed aiming to record 50 cycles for P- and G-type standard (*unmodified*) coin cells between 2.0 and 4.8 V. Four coin cells (denoted G-1-3, G-1-4, P-1-3, P-1-4) were tested at the current corresponding to the 0.2C-rate for all samples. The weight of the active material was 12.01mg, 9.74mg, 10.03mg and 8.25mg for the G-1-3, G-1-4, P-1-3, and P-1-4 coin cells, respectively.

III. RESULTS AND DISCUSSION

A. Synchrotron X-ray Diffraction

To obtain precise crystallographic information about the active materials, synchrotron X-ray powder diffraction was performed. Fig. 2 presents the results obtained from the synchrotron X-ray diffraction analysis on the pristine (labelled as P-type) and graphene-modified (labelled as G-type) $Li[Li_{0.2}Mn_{0.54}Ni_{0.13}Co_{0.13}]O_2$ samples. No significant structural differences were observed between the P-type and G-type active materials, except for small changes in the lattice parameters and atomic positions.
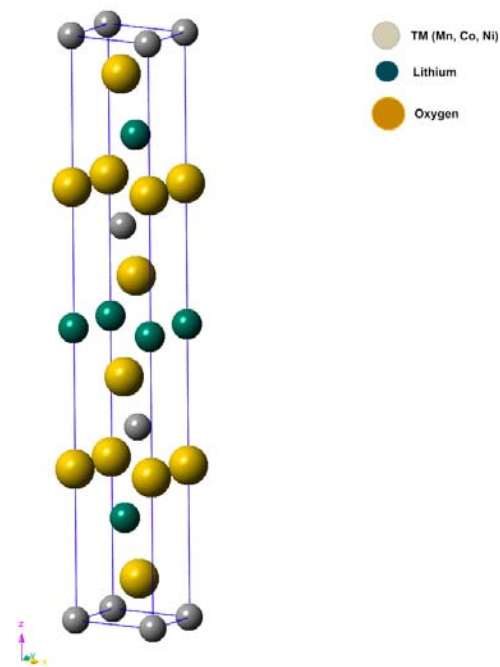
Fig. 1. Crystal structure of LiMO₂ (R-3m) for both P-type and G-type samples, visualised based on GSAS refinement of XRD patterns.

The results obtained from the Rietveld refinement are listed in Table I. The space group was defined as R-3m, which belongs to the trigonal crystal system. The metal occupancy at 3a and 3b sites was refined, as well as the oxygen occupancy at 6c site. Site occupancy of the lithium ion at the 3b site was slightly reduced in the G-type sample.
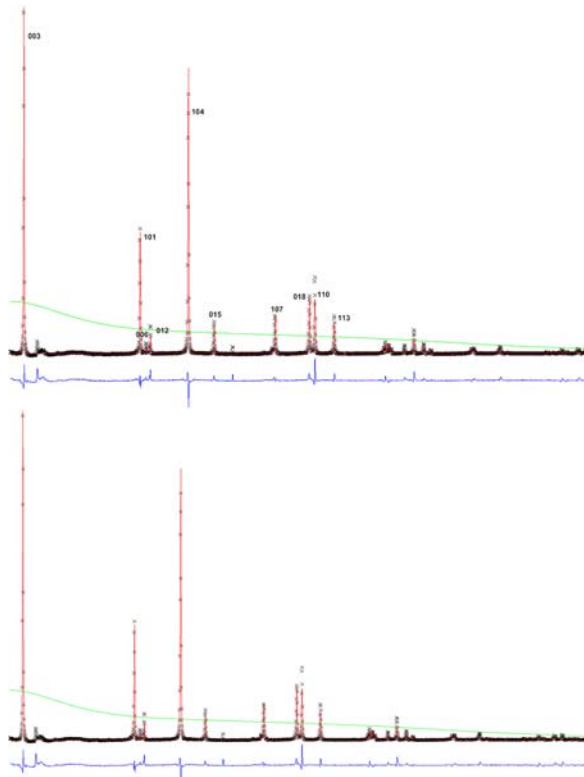
Fig. 2. Synchrotron X-ray diffraction pattern of P-type (pristine) and G-type (graphene-modified) powder of $Li[Li_{0.2}Mn_{0.54}Ni_{0.13}Co_{0.13}]O_2$. Rietveld refinement was performed for the R-3m phase. Measured points are indicated by black crosses. The red line shows the calculated diffraction pattern and the blue line indicates the difference. The X-ray photon energy used for XRD analysis was 11.0 keV (λ = 1.127 Å).

B. Synchrotron X-ray Absorption Spectroscopy

Manganese XANES & EXAFS

X-ray Absorption Near-edge (XANES) spectra can provide insight into the oxidation state of individual atomic species by comparing spectra with reference materials (powders of pure metals or known compounds). Fig. 3 illustrates the normalised X-ray Absorption Near-edge (XANES) spectra of the Mn K edge of powders of $Li[Li_{0.2}Mn_{0.54}Ni_{0.13}Co_{0.13}]O_2$ and the reference cell (G-type).

A number of previous studies [4]-[9] reported changes in the oxidation of transition metals during electrochemical cycling. Mn is believed to exist in the charge state between +3 and +4 in the initial compound. The oxidation state of Co and Ni ions in the initial compound are reported to be trivalent (+3) and divalent (+2), respectively.

The position of the edge is shifted towards higher energies upon charging, and returns to the initial position upon discharging. It has been suggested that the loss of oxygen from the lattice during first charge is irreversible, and is mainly determined by the amount of Li in the transition layer [10]-[11]. During the first charge, the *a* lattice parameter decreases while the *c* parameter increases due to the oxidation of transition metals and the removal of lithium from the intermediate metallic layer within the R-3m structure.

The evaluation of the Mn oxidation state from XANES

TABLE I
RIETVELD REFINEMENT RESULTS FOR THE ACTIVE MATERIALS

Symbol	P-type	G-type
Li-3b		
x	0	0
y	0	0
z	0.5	0.5
Occ.	0.9357	0.8205
Ni-3b		
x	0	0
y	0	0
z	0.5	0.5
Occ.	0.0482	0.0433
Ni-3a		
x	0	0
y	0	0
z	0	0
Occ.	0.1997	0.2987
Mn-3a		
x	0	0
y	0	0
z	0	0
Occ.	0.8719	0.8966
Co-3a		
x	0	0
y	0	0
z	0	0
Occ.	0.1745	0.2863
Li-3a		
x	0	0
y	0	0
z	0	0
Occ.	0.2155	0.2346
O		
x	0	0
y	0	0
z	0.258920	0.259695
Occ.	1.0	1.0
Space Group	R-3m	R-3m
Latt.	A = 2.855754	A = 2.87419
	B = 2.855754	B = 2.87419
	C= 14.257215	C = 14.26741

Occ. = Occupancy, Latt. = Lattice parameter.

spectra requires careful interpretation, since various factors concerned with the structural distortion can also contribute to the change of edge shape.

Detailed *in situ* XAS investigation by Deb et al. [6] revealed that the oxidation states of transition metals were Mn^{4+}, Co^{3+}, and Ni^{2+} in NMC pristine material. It was observed that the oxidation states of the Ni^{2+} and Co^{3+} change into Ni^{4+} and $Co^{4+}(Co^{3.92+})$ upon charging, respectively [4]-[9]. However, some researchers point out that in pristine materials some Mn ions are present in the Mn^{3+} low spin configuration, so that the oxidation state of Mn is +3.75 on average [5],[12]. Future research should therefore concentrate on this issue to investigate the precise oxidation state of Mn that may be related to the ageing mechanism in service.

Double pre-edge peaks were found between 6540 and 6550 eV, as can be seen in Fig. 4. They are sensitive to the geometry of the manganese site and the electronic state. These peaks are related to the 1s-3d transition, and in a centrosymmetric condition those transitions are dipole

forbidden. These peaks appear because of the 3d-4p orbital mixing originating from the loss of centrosymmetry of the slightly distorted octahedral 3a site in the R-3m space group [12]. The intensity of those peaks is strongly dependent on the local symmetry around the core element. High intensity implies more unsymmetrical local environment. As shown in Fig. 4, the *in situ* cell showed stronger peaks compared to the powders.
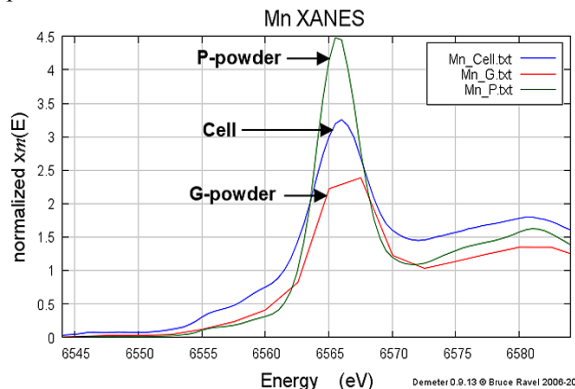
Fig. 3. Normalised XANES spectra at Mn K-edge (6539 eV). Blue curve indicates the reference cell (G-type) and, the red and green curve represents G-type and P-type powder respectively.
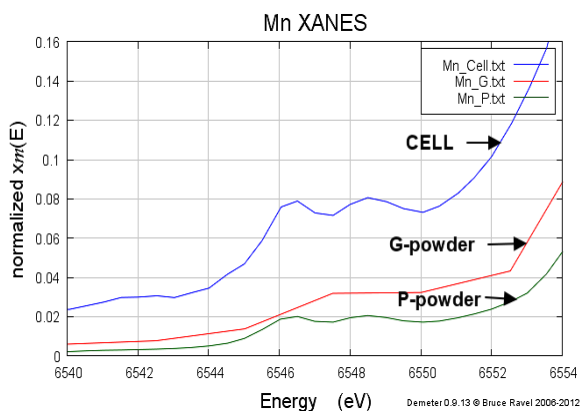
Fig. 4. Double pre-edge peaks of Mn K-edge.

Fig. 5 and Fig. 6 illustrate the Fourier transforms of the Mn EXAFS signal from $Li[Li_{0.2}Mn_{0.54}Ni_{0.13}Co_{0.13}]O_2$ powders (P,G-type) and the reference cell at the Mn K-edge in k-space and R-space respectively. In R-space spectra, the first peak occurs at around R=1.5 Å, although the value for the reference cell is slightly smaller. This peak corresponds to the nearest-neighbour coordination shell of oxygen atoms surrounding Mn (Mn-O). It should be noted that the distance in R-space obtained from the Fourier transform is 0.2-0.5 Å shorter than the actual bond distance due to the energy dependence of phase factors that appear in the expression for the absorption modulation function. The second peak at around 2.4 Å is attributed to transition metal atoms (Mn, Co or Ni) in the second coordination shell (M-M). Lithium atoms are also present in the second coordination shell, but their contribution is below the detection limit. In powder samples, a further peak found at around 3.0 Å is likely to be associated with the O atoms in the third coordination shell.
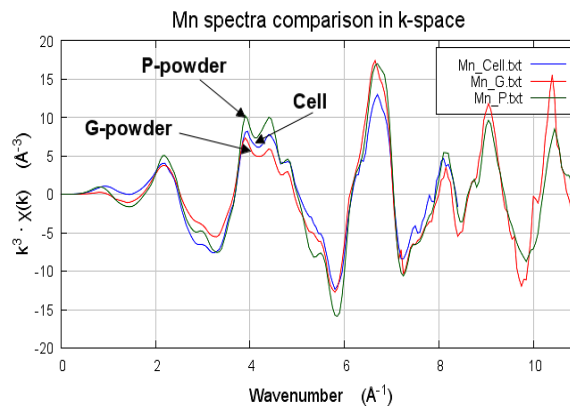
Fig. 5. k^3-weighted Fourier transform in k-space (blue: cell / red: G-type / green: P-type). The spectra have been obtained at the Mn K-edge (6537 eV) of $Li[Li_{0.2}Mn_{0.54}Ni_{0.13}Co_{0.13}]O_2$ powders (P,G-type) and the reference cell.
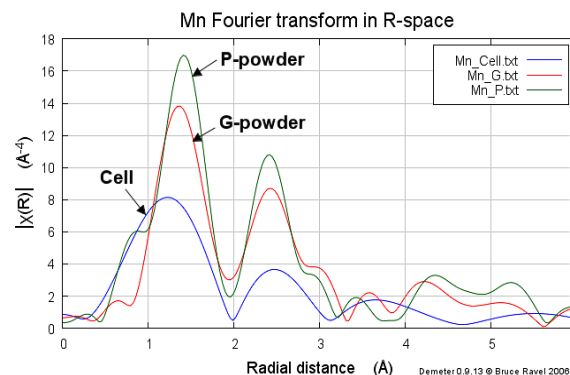
Fig. 6. k^3-weighted Fourier transform in R-space magnitude (blue: cell / red: G-type / green: P-type). The spectra have been obtained at the Mn K-edge (6537 eV) of $Li[Li_{0.2}Mn_{0.54}Ni_{0.13}Co_{0.13}]O_2$ powders (P,G-type) and the reference cell.

Data interpretation was performed with the Demetris software package. Structural parameters were obtained by fitting within the ARTEMIS application with the FEFF 6 algorithm. Crystallographic parameters were first refined by the Rietveld method (GSAS) applied to XRD spectra, and used as the starting values for EXAFS fitting. Atom coordination number was set to 6.0. The EXAFS Debye-Waller factor (denoted by σ^2, and given in brackets for other fit results hereafter) for the Mn-O computation was 0.00561 in the P-type powder sample. Thus, the estimated value of the radial distance (1.897 Å) between Mn and O was arrived at. Another value obtained from the fitting procedure with reasonable confidence was the distance between transition metal atoms, estimated as 2.793 Å (σ^2=0.00833). The atom coordination number of G-type powder was defined as 6.0. The distance between Mn and O was found to be 1.876 Å (σ^2=0.00014) in the graphene-coated sample. As compared to the P-type powder sample, the distance appears shorter. Since similar pristine materials show 1.902 ± 0.011 Å bond lengths between Mn and O [14], the distance between Mn and O in the graphene-coated sample (G-type) appears to deviate from the common value. The Mn-Mn distance was estimated to be 2.778 Å (σ^2=0.00375), also shorter in comparison with the pristine sample.

Nickel XANES & EXAFS

Fig. 7 compares the XANES spectra for the powders and the reference cell at Ni K pre-edge. Highly symmetric Ni structure can be anticipated in the powders. However, a small peak was observed between 8348 eV and 8350 eV in the pre-edge region for the cell. A possible explanation for this peak may be the influence of the electrolyte leak.
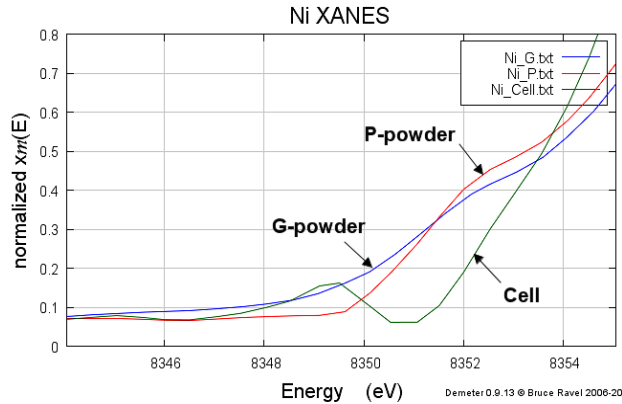
Fig. 7. Pre-edge region of nickel. Green curve indicates the reference cell (G-type) and, the red and blue curve represent G-type and P-type powder respectively.
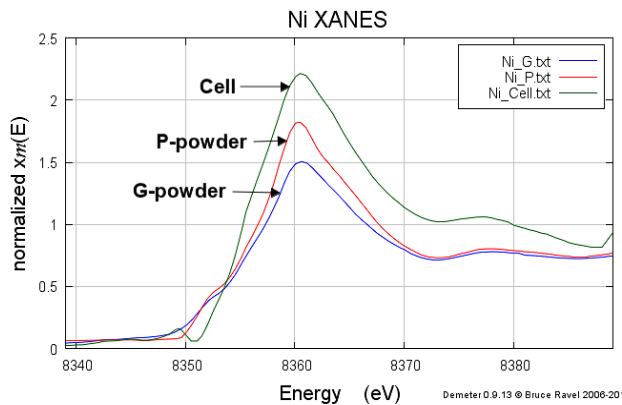
Fig. 8 Normalised XANES spectra at Ni K-edge (8339 eV). Blue curve indicates the reference cell (G-type) and, the red and green curve represent G-type and P-type powder respectively.
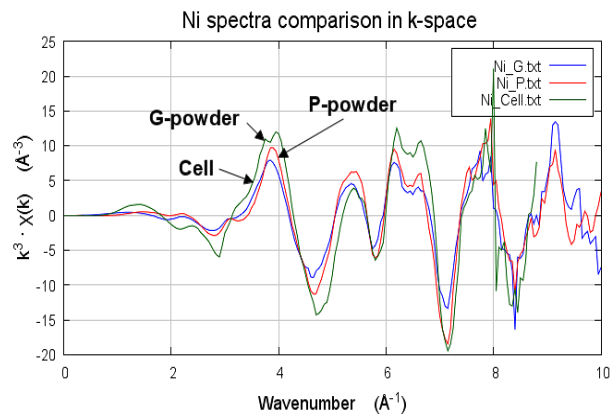
Fig. 9. k^3-weighted Fourier transform in k-space (blue: G-type / red: P-type / green: cell). The spectra have been obtained at the Ni K-edge (8339 eV) of Li[Li$_{0.2}$Mn$_{0.54}$Ni$_{0.13}$Co$_{0.13}$]O$_2$ powders (P,G-type) and the reference cell.
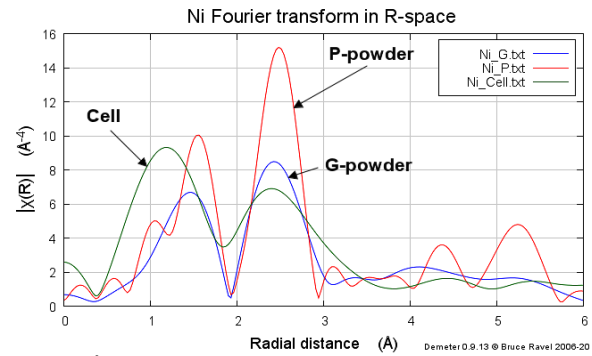
Fig. 10. k^3-weighted Fourier transform in R-space magnitude (blue: G-type / red: P-type / green: cell). The spectra have been obtained at the Ni K-edge (8339 eV) of Li[Li$_{0.2}$Mn$_{0.54}$Ni$_{0.13}$Co$_{0.13}$]O$_2$ powders (P,G-type) and the reference cell.

Normalised XANES spectra collected at the Ni K-edge are shown in Fig. 8. The predominant oxidation state of nickel is +2 in the initial active material. However, during charging-discharging process different oxidation states are expected, such as +3 and +4. The difference in the pre-edge structure of the spectrum between powders and the cell suggests that the geometrical symmetry state of Ni atoms is different.

In the active material, Ni ions can be located at the 3a site, as listed in Table I. During the charging process, the lithium ion is removed from the metal layer, and an oxygen vacancy may occur in the vicinity of nickel ions. This leads to the formation of NiO$_6$ octahedrons. On the other hand, a Ni ion may also be located at the 3b site in the lithium layer. Several studies [15]-[17] have sought to investigate nickel ion migration from the transition metal to lithium layer. This may be clarified further by EXAFS analysis.

Cobalt XANES & EXAFS
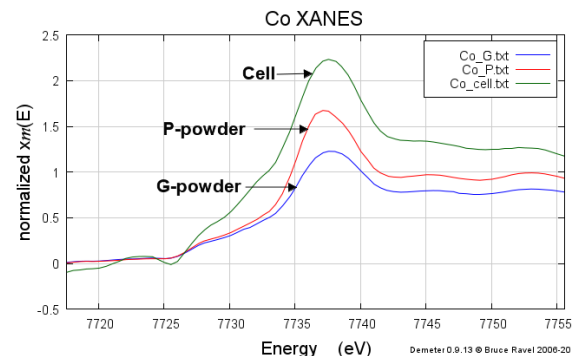
Fig. 11. Normalised XANES spectra at Co K-edge (7712 eV). Green curve indicates the reference cell (G-type) and, the red and blue curve represent P-type and G-type powder respectively.

Normalised XANES spectra at Cobalt K-edge are illustrated in Fig. 11. The oxidation of the cobalt in the active material is known to be +3. The similarity in the XANES spectra at around 7737 eV in Fig. 11 between the powders and the *in situ* cell suggest that the oxidation state of Co remains unchanged with the incorporation in the cell. Generally, cobalt and nickel atoms tend to exist in close proximity as Ni^{3+}Co^{+3} pairs. Due to the presence of the cobalt, the Jahn-Teller distortion from Ni is inhibited during the deintercalation process of lithium. However, the effective

amount of doped Co deserves to be investigated.
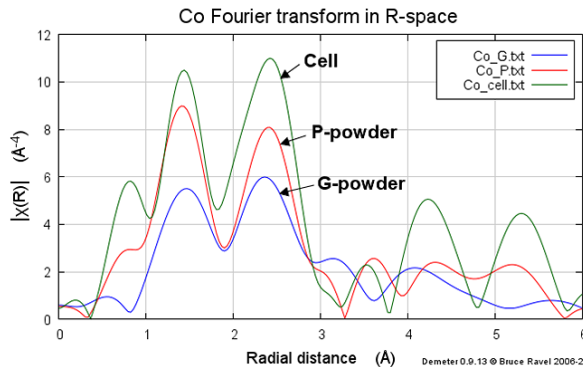
Fig. 12 k^3-weighted Fourier transform in R-space [magnitude part]. The spectra have been obtained at the Co K-edge (7712 eV) of Li[Li$_{0.2}$Mn$_{0.54}$Ni$_{0.13}$Co$_{0.13}$]O$_2$ powders (P,G-type) and the reference cell. The green curve indicates the reference cell, and the blue and the red curve indicates G-type and P-type sample respectively.

EXAFS analysis of Co in the P-type powder sample allowed the evaluation of the distances for Co-O, Co-Ni, and Co-Li coordination shells with high reliability. The radial distance between Co and O was evaluated to be 1.928 Å (σ^2=0.00372), with the atomic coordination number of 6. The distance between two Co atoms occupying two different sites was calculated to be 2.823 Å (σ^2=0.00630), with the same atomic coordination. Interestingly, the presence of Li at the 3b site also showed a scattering effect in the Co spectrum. Based on this calculation, the radial distance was found to be 2.860 Å (σ^2=0.00389), with the atomic coordination number of 6.
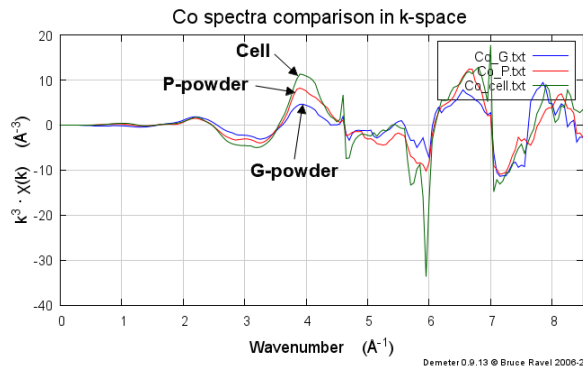
Fig. 13. k^3-weighted Fourier transform in k-space. The spectra have been obtained at the Co K-edge (7712 eV) of Li[Li$_{0.2}$Mn$_{0.54}$Ni$_{0.13}$Co$_{0.13}$]O$_2$ powders (P,G-type) and the reference cell. The green curve indicates the reference cell, and the blue and the red curve indicates G-type and P-type sample respectively.

As to the G-type sample, two atomic-radial distances could be evaluated. The Co-O distance was computed to be 1.955 Å (σ^2=0.00169), and Co-Co was found to be 2.857 Å (σ^2=0.00026). According to the fitting result, there was a significant difference between the two powder types. Previous research findings into the radial distance between the Co and O in similar pristine materials [17] reported the distance of 1.919 Å, a similar value (1.928 Å) found for the P-type in this experiment. However, the Co-O distance of 1.955 Å measured for the G-type powder appears to be increased. This effect deserves further analysis.

C. Galvanostatic Tests

Galvanostatic charging-discharging tests for the coin cells G-1-3, G-1-4, P-1-3, and P-1-4 (active material loading of 12.01mg, 9.74mg, 10.03mg and 8.25mg, respectively) were performed between 2.0 and 4.8 V at the charge rate of 0.2C.
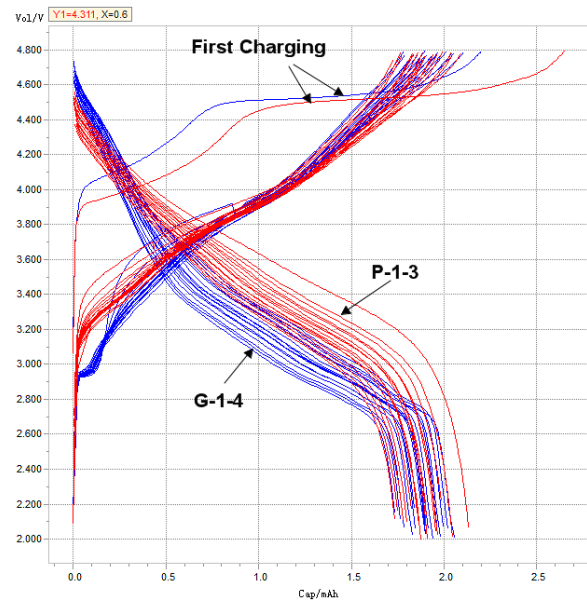
Fig. 14. The galvanostatic profiles (20 cycles) of G-1-4 (blue curves) and P-1-3 (red curves) coin cells at 0.2C-rate in a voltage range of 2.0-4.8 V.

Fig. 14 compares the galvanostatic profiles for G-1-4 and P-1-3 coin cells, and Fig. 15 reports the results for G-1-3 and P-1-4 coin cells. The efficiency from the first cycle was 93.28% and 80.64% for the G-1-4 and P-1-3 cells respectively.
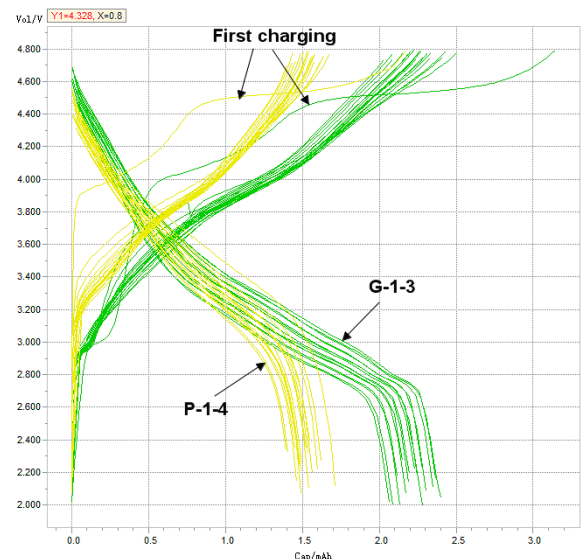
Fig. 15. The galvanostatic profiles (20 cycles) of G-1-3 (green curves) and P-1-4 (yellow curves) coin cells at 0.2C-rate in a voltage range of 2.0-4.8 V.

Afterwards, both samples showed high efficiency ranging from 96% to 100%. It is apparent from this data that the graphene-coated cell showed better performance until 20 cycles. As can be seen from the galvanostatic profile in Fig. 15, the computed efficiency from the first cycle was 76.7%

and 79.24% for the G-1-3 and P-1-4 cells respectively.

Clear indication of cell degradation emerge from the galvanostatic profiles between 21 and 50 cycles, as shown in Fig. 16. It is apparent that G-type coin cells reveal shorter life-span than P-type coin cells. While G-1-4 performance fades from 24th cycle onwards, the performance of P-type samples typically remain steady until the 40th cycle.
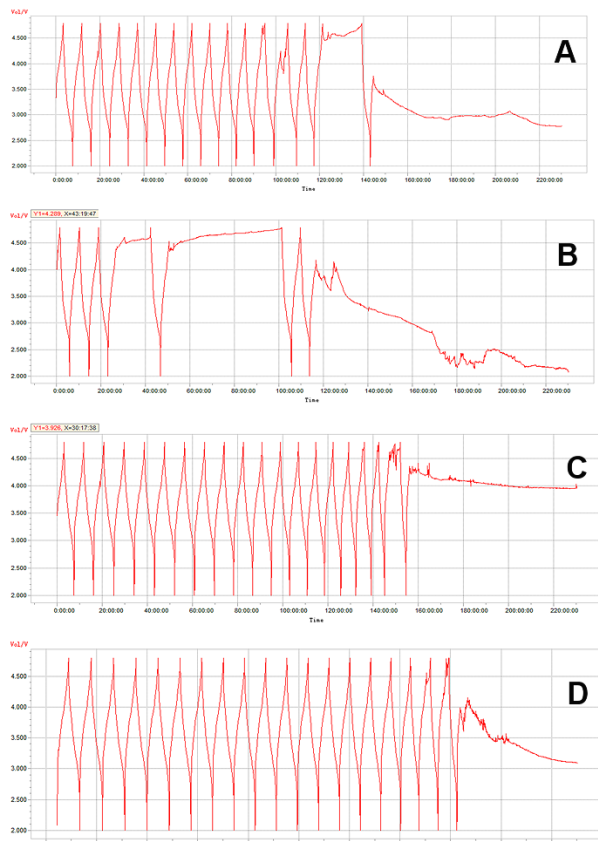
Fig. 16. The galvanostatic profiles (between 21 and 50 cycles) of G-1-3 (A), G-1-4 (B), P-1-3 (C), and P-1-4 (D) coin cells at 0.2C-rate in a voltage range of 2.0-4.8 V. Y axis is the voltage (V) and X axis is the time.

D. Conclusion

This study has shown that the XAS method has a great potential to examine the ageing mechanism of the NMC based lithium-ion batteries. X-ray diffraction approaches can provide average information about the crystal structure. However, in lithium-ion batteries, the capacity and stability of the active material depend not only on the periodic crystal lattice, but also on the local environment of individual atoms. In this respect, XAS appears to have sensitivity sufficient for the investigation of atomic re-arrangement phenomena that are likely to be associated with capacity fading mechanisms. The findings of this study also have a number of important implications for *in operando* study of the electrode degradation in lithium-ion batteries.

REFERENCES

[1] Armand, M. and Tarascon, J.M. (2008), "Building better batteries," Nature, Vol. 451 No. 7179, pp. 652–657.

[2] Jarvis, K.A., Deng, Z., Allard, L.F., Manthiram, A. and Ferreira, P.J. (2011), "Atomic Structure of a Lithium-Rich Layered Oxide Material for Lithium-Ion Batteries: Evidence of a Solid Solution," Chemistry of Materials, Vol. 23 No. 16, pp. 3614–3621.

[3] Zheng, J., Deng, S., Shi, Z., Xu, Hongjie, Xu, Hui, Deng, Y., Zhang, Z., et al. (2013), "The effects of persulfate treatment on the electrochemical properties of $Li[Li0.2Mn0.54Ni0.13Co0.13]O2$ cathode material," Journal of Power Sources, Vol. 221, pp. 108–113.

[4] Croy, J.R., Balasubramanian, M., Kim, D., Kang, S.-H. and Thackeray, M.M. (2011), "Designing High-Capacity, Lithium-Ion Cathodes Using X-ray Absorption Spectroscopy," Chemistry of Materials, Vol. 23 No. 24, pp. 5415–5424.

[5] Ito, A., Sato, Y., Sanada, T., Hatano, M., Horie, H. and Ohsawa, Y. (2011), "In situ X-ray absorption spectroscopic study of Li-rich layered cathode material Li [Ni0.17Li0.2Co0.07Mn0.56]O2," Journal of Power Sources, Vol. 196 No. 16, pp. 6828–6834.

[6] Deb, A., Bergmann, U., Cramer, S.P. and Cairns, E.J. (2005), "In situ x-ray absorption spectroscopic study of the Li[Ni 1/3Co1/3Mn1/3]O2 cathode material," Journal of Applied Physics, Vol. 97 No. 11, p. 113523.

[7] Kim, J.M. and Chung, H.T. (2004), "Role of transition metals in layered Li [Ni, Co, Mn]O2 under electrochemical operation," Electrochimica Acta, Vol. 49 No. 21, pp. 3573–3580.

[8] Johnson, C.S., Li, N., Lefief, C. and Thackeray, M.M. (2007), "Anomalous capacity and cycling stability of xLi2MnO3•(1−x)LiMO2 electrodes (M=Mn, Ni, Co) in lithium batteries at 50°C," Electrochemistry Communications, Vol. 9 No. 4, pp. 787–795.

[9] Kim, G.-Y., Yi, S.-B., Park, Y.J. and Kim, H.-G. (2008), "Electrochemical behaviors of Li[Li(1−x)/3Mn(2−x)/3Nix/3Cox/3]O2 cathode series (0<x<1) synthesized by sucrose combustion process for high capacity lithium ion batteries," Materials Research Bulletin, Vol. 43 No. 12, pp. 3543–3552.

[10] Jiang, M., Key, B., Meng, Y.S. and Grey, C.P. (2009), "Electrochemical and Structural Study of the Layered, 'Li-Excess' Lithium-Ion Battery Electrode Material Li[Li1/9Ni1/3Mn5/9]O2," Chemistry of Materials, Vol. 21 No. 13, pp. 2733–2745.

[11] Zhang, X., Yu, C., Huang, X., Zheng, J., Guan, X., Luo, D. and Li, L. (2012), "Novel composites Li[LixNi0.34−xMn0.47Co0.19]O2 (0.18 ≤ x ≤ 0.21): Synthesis and application as high-voltage cathode with improved electrochemical performance for lithium ion batteries," Electrochimica Acta, Vol. 81, pp. 233–238.

[12] Simonin, L., Colin, J.-F., Ranieri, V., Canévet, E., Martin, J.-F., Bourbon, C., Baehtz, C., et al. (2012), "In situ investigations of a Li-rich Mn–Ni layered oxide for Li-ion batteries," Journal of Materials Chemistry, Vol. 22 No. 22, p. 11316.

[13] Yoon, W.-S., Paik, Y., Yang, X.-Q., Balasubramanian, M., McBreen, J. and Grey, C.P. (2002), "Investigation of the Local Structure of the LiNi0.5Mn0.5 O 2 Cathode Material during Electrochemical Cycling by X-Ray Absorption and NMR Spectroscopy," Electrochemical and Solid-State Letters, Vol. 5 No. 11, pp. A263–A266.

[14] Ito, A., Sato, Y., Sanada, T., Hatano, M., Horie, H. and Ohsawa, Y. (2011), "In situ X-ray absorption spectroscopic study of Li-rich layered cathode material Li[Ni0.17Li0.2Co0.07Mn0.56]O2," Journal of Power Sources, Vol. 196 No. 16, pp. 6828–6834.

[15] He, P., Yu, H., Li, D. and Zhou, H. (2012), "Layered lithium transition metal oxide cathodes towards high energy lithium-ion batteries," Journal of Materials Chemistry, Vol. 22 No. 9, p. 3680.

[16] Yabuuchi, N., Yoshii, K., Myung, S.-T., Nakai, I. and Komaba, S. (2011), "Detailed Studies of a High-Capacity Electrode Material for Rechargeable Batteries, Li2MnO3−LiCo1/3Ni1/3Mn1/3O 2," Journal of the American Chemical Society, Vol. 133 No. 12, pp. 4404–4419.

[17] Croy, J.R., Balasubramanian, M., Kim, D., Kang, S.-H. and Thackeray, M.M. (2011), "Designing High-Capacity, Lithium-Ion Cathodes Using X-ray Absorption Spectroscopy," Chemistry of Materials, Vol. 23 No. 24, pp. 5415–5424.